Geoderma 438 (2023) 116631

Contents lists available at ScienceDirect

Geoderma

journal homepage: www.elsevier.com/locate/geoderma

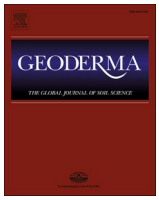

Robust calibration and evaluation of a percolation-based effective-medium approximation model for thermal conductivity of unsaturated soils

Yongwei Fu [a], Behzad Ghanbarian [b], Robert Horton [c], Joshua Heitman [a,*]

[a] Department of Crop & Soil Sciences, North Carolina State University, Raleigh 27695, United States
[b] Department of Geology, Porous Media Research Lab, Kansas State University, Manhattan 66506, United States
[c] Department of Agronomy, Iowa State University, Ames 50011, United States

ARTICLE INFO

Handling Editor: L. Morgan Cristine

Keywords:
Percolation-based effective-medium approximation
Saturation
Thermal conductivity
Water content

ABSTRACT

Thermal conductivity (λ) is a property characterizing heat transfer in porous media, such as soils and rocks, with broad applications to geothermal systems and aquifer characterizations. Numerous empirical and physically-based models have been developed for thermal conductivity in unsaturated soils. Recently, Ghanbarian and Daigle (G&D) proposed a theoretical model using the percolation-based effective-medium approximation. An explicit form of the G&D model relating λ to water content (θ) and equations to estimate the model parameters were also derived. In this study, we calibrated the G&D model and two widely applied empirical λ(θ) models using a robust calibration dataset of 41 soils. All three λ(θ) model performances were evaluated using a validation dataset of 58 soils. After calibration, the root mean square error (RMSE), mean absolute error (MAE) and coefficient of determination (R^2) of the G&D model were 0.092 W^{-1} m^{-1} K^{-1}, 0.067 W^{-1} m^{-1} K^{-1} and 0.97, respectively. For the two empirical models, RMSEs ranged from 0.086 to 0.096 W^{-1} m^{-1} K^{-1}, MAEs from 0.063 to 0.071 W^{-1} m^{-1} K^{-1}, and R^2 values were about 0.97. All three metrics indicated that calibration improved the performance of the G&D model, and it had an accuracy similar to that of the two empirical λ(θ) models. Such a robust performance confirmed that the theoretically-based G&D model can be applied to study soil heat transfer and potentially other related fields.

1. Introduction

Thermal conductivity (λ) is an important property involved with heat conduction in soils. It is defined as the coefficient between heat flux under steady state conditions and temperature gradient through the macroscopic Fourier equation. Generally, soil thermal conductivity is affected by various physical properties, such as bulk density, porosity (ϕ), particle size distribution, soil structure, temperature, and especially water content (θ) (Shiozawa and Campbell, 1990; Abu-Hamdeh and Reeder, 2000; Usowicz et al., 2013).

Because of the dominant role that θ plays in moderating λ, a large number of λ(θ) models are available to estimate the thermal conductivity of unsaturated soils. Roughly, these models can be classified into two major categories: (1) empirical and (2) physically-based. Empirical models are typically developed based on the flexibility of a mathematical equation to produce the correct trend in observed values. Various empirical thermal conductivity models have been proposed (e.g., Johansen, 1975; Côté and Konrad, 2005a; Lu et al., 2007; Chen, 2008; He et al., 2017; Zhao et al., 2019). However, model parameters are unknown a priori, and their physical meanings are not fully clear. Model parameters can be determined by directly fitting the model to observations. Optimized parameters are database-dependent, meaning that they may not be ideal for use on soil types not included in the optimization process. Some physically-based models consider different components, such as solids and fluids contributing to thermal conductivity in a combination of series and parallel in the cubic cell or representative elementary volume (de Vries, 1963; Tong et al., 2009). Some others provide a different but relatively close configuration to that of a real soil in order to simulate heat transfer within soil (i.e., they usually assume one dimensional heat transfer) (Gori and Corasaniti, 2013; Haigh, 2015). However, these models are either over-simplified in comparison to real soil micro-structures (i.e., particle geometry, particle/pore size distribution, pore-water arrangement, and interfacial properties) or are in a complex form, which makes it difficult to determine their parameters, and thus they lack prediction accuracy (Dong et al., 2015; Jia et al., 2019).

* Corresponding author.
E-mail address: jlheitma@ncsu.edu (J. Heitman).

https://doi.org/10.1016/j.geoderma.2023.116631
Received 14 October 2022; Received in revised form 23 February 2023; Accepted 3 August 2023
Available online 8 August 2023

One of the theoretical thermal conductivity models is based on the percolation-based effective-medium approximation presented by Ghanbarian and Daigle (2016) (hereafter G&D model). Ghanbarian and Daigle (2016) explicitly derived θ as a function of λ, and showed that their theoretical model reasonably well described fine- and coarse-textured soil observations. Then, Sadeghi et al. (2018) presented an explicit λ(θ) form of the G&D model and demonstrated that the G&D model could reduce to other existing λ(θ) models as its special cases (section 4 in their study). Sadeghi et al. (2018) also proposed regression-based relationships to estimate parameters of the G&D model using the clay content of a soil.

Compared to other models, the G&D model has three main advantages: (i) its parameters are physically meaningful, (ii) two parameters can be easily estimated from clay content using linear relationships, and (iii) independent validation on four sand packs demonstrate its reliability. Thus, the G&D model appears to provide the potential for broad usage in predicting soil heat transfer. However, the linear regressions proposed by Sadeghi et al. (2018) are based on only 17 soil samples and show limitations because of using only clay content as an input (shown later in section 2.1), thus more robust model calibration and validation for additional soils are warranted.

The objectives of this study, therefore, are to calibrate and validate the G&D model using a broader range and larger number of soils and obtain best-fitting parameters for three textural groups, then compare the calibrated G&D model results to those derived from two widely used empirical λ(θ) models.

2. Materials and methods

2.1. Percolation-based effective-medium approximation model

Using concepts of the percolation-based effective-medium approximation (McLachlan, 1987), Ghanbarian and Daigle (2016) developed the following theoretical relationship to model thermal conductivity in unsaturated soils

$$(\phi-\theta)\frac{\lambda_{dry}^{1/t_s}-\lambda^{1/t_s}}{\lambda_{dry}^{1/t_s}+[(\phi-\theta_c)/\theta_c]\lambda^{1/t_s}}+\theta\frac{\lambda_{sat}^{1/t_s}-\lambda^{1/t_s}}{\lambda_{dry}^{1/t_s}+[(\phi-\theta_c)/\theta_c]\lambda^{1/t_s}}=0 \quad (1)$$

Eq. (1) can be rewritten to implicitly link thermal conductivity λ to water content θ

$$\theta=\frac{\left[\lambda^{1/t_s}-\lambda_{dry}^{1/t_s}\right]\left[\theta_c\lambda_{sat}^{1/t_s}+(\phi-\theta_c)\lambda^{1/t_s}\right]}{\left[\lambda_{sat}^{1/t_s}-\lambda_{dry}^{1/t_s}\right]\lambda^{1/t_s}} \quad (2)$$

where λ_{dry} and λ_{sat} are thermal conductivity at dry and saturated soil conditions, respectively, t_s is the scaling exponent, and θ_c is the critical water content at which the high-conductivity component first forms a continuous percolation path (i.e., water capillary bridges surrounding grain-grain contacts).

Sadeghi et al. (2018) derived an explicit λ(θ) form of the G&D model:

$$\lambda=\left[b_1+b_2\theta+\mathrm{sgn}(t_s)b_2\sqrt{b_3+2b_1b_2^{-1}\theta+\theta^2}\right]^{t_s} \quad (3)$$

where sgn is the sign function (i.e., $\mathrm{sgn}(t_s>0)=1$, $\mathrm{sgn}(t_s<0)=-1$) and

$$b_1=\frac{-\theta_c\lambda_{sat}^{1/t_s}+(\theta_s-\theta_c)\lambda_{dry}^{1/t_s}}{2(\theta_s-\theta_c)} \quad (4a)$$

$$b_2=\frac{\lambda_{sat}^{1/t_s}-\lambda_{dry}^{1/t_s}}{2(\theta_s-\theta_c)} \quad (4b)$$

$$b_3=\frac{\left[\theta_c\lambda_{sat}^{1/t_s}-(\theta-\theta_c)\lambda_{dry}^{1/t_s}\right]^2+4\theta_c(\theta_s-\theta_c)\lambda_{sat}^{1/t_s}\lambda_{dry}^{1/t_s}}{\left(\lambda_{sat}^{1/t_s}-\lambda_{dry}^{1/t_s}\right)^2} \quad (4c)$$

Theoretically, $t_s>0$, and, thus, the sign function in Eq. (3) can be eliminated. Sadeghi et al. (2018) proposed two regression-based relationships to estimate t_s and θ_c from clay content (f_{clay}) based on 17 soil samples with clay contents ranging from 0.01 to 0.43:

$$\theta_c=0.33f_{clay} \quad (5)$$

$$t_s=-0.25f_{clay}+0.342 \quad (6)$$

In combination with Eqs. (5) and (6), Sadeghi et al. (2018) used the G&D model to successfully estimate λ values of four sand packs. However, further assessments are required using a wider range of soils to support the model's applicability. Furthermore, Eqs. (5) and (6) are derived using only 17 soil samples and, thus, they are not expected to accurately estimate θ_c and t_s values and accordingly saturation-dependent thermal conductivity for all soil types, particularly those with clay contents>0.43.

Eqs. (5) and (6) use clay content as the only predictor, which introduces some issues at both low and high clay contents. When f_{clay} is low (e.g., < 0.1), the estimated λ(θ) curve by Eqs. (4)-(6) shows typical characteristics of sandy soils: less pronounced 'flat tail' behavior and sharp increase in the pendular regime (Fig. 1). Thus, the G&D model is expected to perform well on sandy soils (e.g., four sand packs as reported by Sadeghi et al. (2018)) but poorly for finer-textured soils with similar f_{clay}. For example, Soils 2 and 26 have the same f_{clay} (i.e., 0.06), but the former is a sand soil and the latter is a silt loam soil. Figure 2 presents the thermal conductivity versus the water content curves using Eqs. (4)-(6) on these two soils. Obviously, the G&D model can capture the λ(θ) curve trend for Soil 2, but λ was overestimated particularly in the low θ range for Soil 26. As the f_{clay} increases, the θ_c increases but t_s decreases. Thus, the estimated λ(θ) curves by Eqs. (4)-(6) have more pronounced flat regions at low saturation values but drastic increases at medium saturation values with high clay content (Fig. 1). The curve at high f_{clay} (e.g., 0.5), however, does not mimic those of coarse-textured or fine-textured soils: the former has a rapid increase of λ with increasing θ but a less pronounced flat tail at low θ, whereas the latter has more static behavior at the dry end and also a more gradual λ response as θ increases. Therefore, it is necessary to calibrate and validate the G&D model using a large number of soils and develop new equations, in place of Eqs. (5)

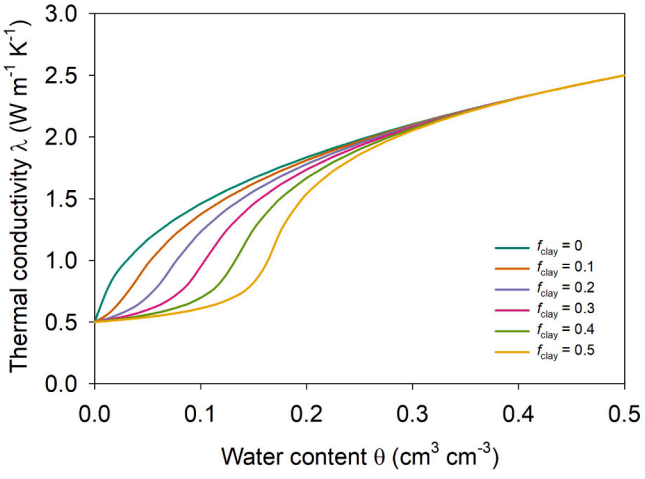

Fig. 1. Thermal conductivity, λ, as a function of water content, θ, determined via the G&D model (equation 4) for various clay contents (f_{clay}). The θ_c and t_s model parameters are estimated from f_{clay} using Eqs. (5) and (6), respectively. We set $\lambda_{dry}=0.5$ W m^{-1} K^{-1} and $\lambda_{sat}=2.5$ W m^{-1} K^{-1}.

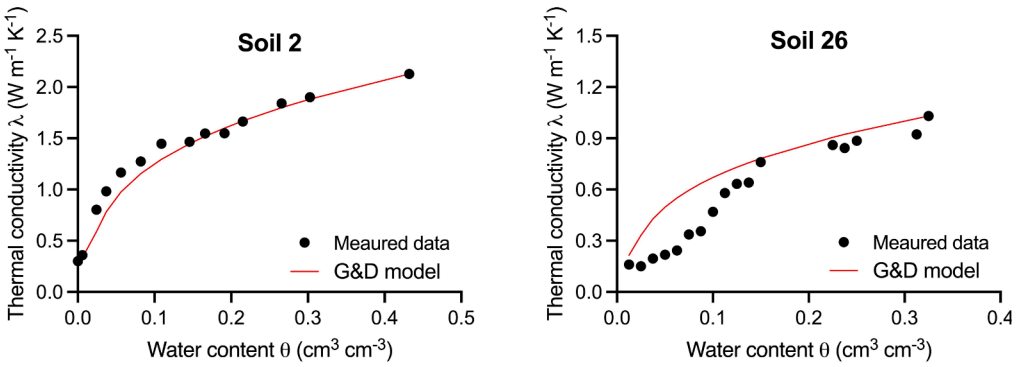

Fig. 2. Thermal conductivity, λ, as a function of water content, θ, determined via the G&D model (equation 4) for Soils 2 and 26. The θ_c and t_s model parameters are estimated from f_{clay} using Eq. (5) and (6), respectively.

and (6), to estimate t_s and θ_c.

2.2. *Côté and Konrad (2005a) model*

Côté and Konrad (2005a) proposed a hyperbolic equation incorporating a texture-dependent parameter κ that relates λ to saturation S_r as follows:

$$K_e = \frac{\lambda - \lambda_{dry}}{\lambda_{sat} - \lambda_{dry}} = \frac{\kappa S_r}{1 + (\kappa - 1)S_r} \tag{7}$$

where K_e is the normalized thermal conductivity, and S_r is water saturation. Using data of 10 soil samples reported by Kersten (1949), Côté and Konrad (2005a) found κ = 3.55 for medium and fine sands and 1.90 for silty and clayey soils.

2.3. *Lu et al. (2007) model*

To address the tail behavior of λ(*S*) curves at low S_r for fine-textured soils, Lu et al. (2007) established an exponential λ equation in terms of S_r:

$$K_e = \frac{\lambda - \lambda_{dry}}{\lambda_{sat} - \lambda_{dry}} = \exp\left\{\alpha\left[1 - S_r^{(\alpha-\beta)}\right]\right\} \tag{8}$$

where α and β are two empirical parameters. Lu et al. (2007) divided eight soil samples into two groups according to their sand contents (f_{sand}): (i) four coarse-textured soils (i.e., $f_{sand} \geq 0.4$) and (ii) four fine-textured soils (i.e., $f_{sand} < 0.4$). By directly fitting Eq. (8) to the samples, they found α values of 0.96 and 0.27 for coarse- and fine-textured soils, respectively. β, another empirical parameter in Eq. (8), was reported to be 1.33.

2.4. *Datasets*

In this study, data representing 99 soils were collated from the literature to calibrate and independently validate the G&D, Côté and Konrad (2005a) (hereafter C&K), and Lu et al. (2007) (hereafter Lu) models. All of the soils satisfied the following criteria: (1) data collection was via reliable experimental techniques (details can be found in associated publications) and setup at room temperature (i.e., 20–25 °C, as temperature effects were not be considered in this study); (2) at least five measured values on the λ-θ curve from dryness to saturation (with sigmoidal shape) were available; (3) complete information, such as sand, silt, and clay contents (f_{sand}, f_{silt} and f_{clay}) and porosity (ϕ), was known for all samples. Measured λ_{dry} and λ_{sat} values were required inputs for the three models. If they were not available, they were indirectly estimated from soil quartz content (f_{quartz}) and porosity (ϕ) using the following relationships proposed by Johansen (1975) and Lu et al. (2007), respectively:

$$\lambda_{sat} = \left(\lambda_q^{f_{quartz}} \lambda_o^{1-f_{quartz}}\right)^{1-\phi} \lambda_w^{\phi} \tag{9}$$

$$\lambda_{dry} = -0.56\phi + 0.51 \tag{10}$$

where λ_q is the thermal conductivity of quartz (7.7 W m^{-1} K^{-1}), and λ_o is the thermal conductivity of other minerals and equal to 2.0 W m^{-1} K^{-1}, when $f_{quartz} > 0.2$, and 3.0 W m^{-1} K^{-1}, when $f_{quartz} \leq 0.2$.

Eq. (9) is based on the geometric mean method, which can only give reliable estimates when the ratio of λ_s/λ_w is<10 (Woodside and Messmer, 1961; Côté and Konrad, 2005a; Tarnawski and Leong, 2016). For most soil minerals, λ_s ranges from 1.8 to 8.8 W m^{-1} K^{-1} (Horai, 1971) and thermal conductivity of water (λ_w) is 0.598 W m^{-1} K^{-1} at 20 °C. Thus, it is unsurprising that Eq. (9) has been extensively used in empirical thermal conductivity models (Donazzi et al., 1979; Lu et al., 2007; Chen, 2008; He et al., 2017), and its reliability on estimating the λ_{sat} also has been tested (Woodside and Messmer, 1961; Johansen, 1975; Tarnawski et al., 2018; Wang et al., 2020) when quartz content is available and used. Dry soils can be regarded as a mixture of soil solids and air, and λ_s is dominant compared to thermal conductivity of air (0.025 W m^{-1} k^{-1}). For such a case, the geometric mean method is no longer valid, and various models to estimate the λ_{dry} with porosity or bulk density as indicators have thus been proposed. He et al. (2021a) reviewed 48 models for estimating the λ_{dry} and found that Eq. (10) was one of the best performing models with RMSE of 0.09 W m^{-1} K^{-1} (i.e., lowest among all models), Nash-Sutcliff Efficiency (NSE) of 0.40 (i.e., 17th among all models) and Akaike information criterion (AIC) of -3103 (i.e., 7th among all models). Therefore, Eqs. (9) and (10) were used to indirectly estimate the λ_{dry} and λ_{sat} values for the soils that did not have directly measured values.

The 99 soils were then divided into a calibration dataset of 41 soils (Soils 1–41), listed in Table 1, and a validation dataset of 58 soils (Soils 42–99), listed in Table 2, to ensure that both groups covered a variety of soil textures (Fig. 3), which was a major factor controlling the λ-θ curves. Note that Soils 1–8, Soils 1–13 and Soils 15–24 in the calibration dataset were used, respectively, to determine the α value for coarse- and fine-textured soils by Lu et al. (2007), to develop Eqs. (5) and (6) by Sadeghi et al. (2018) and to fit the parameter κ for medium and fine sands and silty and clayey soils by Côté and Konrad (2005a). For a thorough and fair comparison, we used a relatively large dataset consisting of more than these 23 soils to calibrate texture-dependent α and κ values and to develop improved relationships for t_s and θ_c. Tables 1 and 2 present the basic soil physical properties and the sources of the 99 soils.

2.5. *Fitting model parameters to thermal conductivity data*

Three models were fitted to the λ(θ) (or λ(*S*)) measurements with a

Table 1
Soil ID, texture, particle size distribution, quartz content, porosity (ϕ) and sources of soils in the calibration dataset including 41 soil samples. The star symbol represents the sum of gravel and sand contents. The hash symbol represents soil samples having no λ_{dry} or λ_{sat} values measured.

Soil ID	Texture	Particle size distribution			Quartz content	ϕ	Sources
		Sand	Silt	Clay		$cm^3\ cm^{-3}$	
1	sand	0.94	0.01	0.05	–	0.40	Lu et al. (2007)
2	sand	0.93	0.01	0.06	–	0.40	Lu et al. (2007)
3	sandy loam	0.67	0.21	0.12	–	0.48	Lu et al. (2007)
4	loam	0.40	0.49	0.11	–	0.55, 0.51, 0.47	Lu et al. (2007)
5	silt loam	0.27	0.51	0.22	–	0.50	Lu et al. (2007)
6	silt loam	0.11	0.70	0.19	–	0.51	Lu et al. (2007)
7	silty clay loam	0.19	0.54	0.27	–	0.55, 0.51, 0.47	Lu et al. (2007)
8	silty clay loam	0.08	0.60	0.32	–	0.51	Lu et al. (2007)
9	clay loam	0.32	0.38	0.30	–	0.51	Lu et al. (2007)
10	loam	0.50	0.41	0.09	–	0.48	Lu et al. (2007)
11	sand	0.92	0.07	0.01	–	0.40	Lu et al. (2007)
12	silty clay	0.07	0.50	0.43	–	0.52	Lu et al. (2011)
13	sand	0.94	0.01	0.05	–	0.40	Lu et al.(2013)
14	silt loam	0.02	0.73	0.25	–	0.55	Lu et al. (2007)
15	sand#	0.97*	0.03	0.00	0.12	0.33–0.43	Kersten (1949)
16	sand#	1.00*	0.00	0.00	0.08	0.34–0.46	Kersten (1949)
17	sand#	1.00	0.00	0.00	0.72	0.30–0.46	Kersten (1949)
18	sand#	1.00	0.00	0.00	0.99	0.35–0.42	Kersten (1949)
19	clay#	0.02	0.20	0.78	0.23	0.33–0.60	Kersten (1949)
20	silty clay loam#	0.09	0.64	0.27	0.05	0.40–0.66	Kersten (1949)
21	silt loam#	0.08	0.81	0.11	0.13	0.35–0.58	Kersten (1949)
22	sandy loam#	0.69*	0.21	0.10	0.59	0.20–0.50	Kersten (1949)
23	sandy loam#	0.54*	0.28	0.18	0.51	0.25–0.48	Kersten (1949)
24	silt loam#	0.22*	0.64	0.14	0.02	0.32–0.56	Kersten (1949)
25	sand#	0.95	0.03	0.02	0.63	0.43	McInnes (1981)
26	silt loam#	0.30	0.64	0.06	0.42	0.53	McInnes (1981)
27	silt loam#	0.30	0.61	0.09	0.42	0.53	McInnes (1981)
28	silt loam#	0.20	0.68	0.12	0.38	0.53	McInnes (1981)
29	silt loam#	0.20	0.57	0.23	0.45	0.53	McInnes (1981)
30	sand#	0.89	0.06	0.05	0.61	0.43	Campbell et al. (1994)
31	silt loam#	0.20	0.55	0.25	0.38	0.55	Campbell et al. (1994)
32	silt loam#	0.11	0.68	0.21	0.36	0.52	Campbell et al. (1994)
33	silty clay#	0.09	0.44	0.47	0.35	0.57	Campbell et al. (1994)
34	sandy loam#	0.54	0.32	0.15	0.49	0.49	Campbell et al. (1994)
35	silt loam#	0.19	0.59	0.23	0.38	0.59	Campbell et al. (1994)
36	silt loam#	0.23	0.63	0.14	0.39	0.53	Campbell et al. (1994)
37	silt loam#	0.17	0.70	0.13	0.00	0.71	Campbell et al. (1994)
38	sandy loam#	0.75	0.10	0.15	0.56	0.41	Hopmans and Dane (1986)
39	sand	1.00	0.00	0.00	1.00	0.32, 0.40	Tarnawski et al. (2013)
40	sand	1.00	0.00	0.00	1.00	0.32	Tarnawski et al. (2013)
41	sand	1.00	0.00	0.00	0.88	0.38, 0.40	Tarnawski et al. (2013)

least squares method by minimizing the following objective function:

$$O_\lambda(p) = \sum_{i=1}^{N_\lambda} \left(\lambda_i - \lambda_i^{'}\right)^2 \tag{11}$$

where λ_i and $\lambda_i^{'}$ are the measured and fitted thermal conductivity values, respectively, N_λ is the number of measured $\lambda(\theta)$ (or $\lambda(S)$) data points in each group and p are the parameter vectors, which are {κ} for the C&K model, {α, β} for the Lu model, and {θ_c, t_s} for the G&D model.

2.6. Statistical analysis

In this study, we compared the estimated λ values via different models with the measured λ values. The model performances were evaluated using: (1) root mean square error (RMSE) describing the spread of the errors around the measured λ values, and a value of 0 indicates a perfect model estimation; (2) mean absolute error (MAE) describing the average absolute errors, and MAE = 0 indicates a perfect model estimation; and (3) coefficient of determination (R^2) describing how well observed outcomes are replicated by the model, and a R^2 value of unity indicates the model values perfectly match the measured values.

$$\mathrm{RMSE} = \sqrt{\frac{\sum \left(\lambda_{\mathrm{estimated}} - \lambda_{\mathrm{measured}}\right)^2}{N}} \tag{12}$$

$$\mathrm{MAE} = \frac{\sum |\lambda_{\mathrm{estimated}} - \lambda_{\mathrm{measured}}|}{N} \tag{13}$$

$$R^2 = 1 - \frac{\sum \left(\lambda_{\mathrm{estimated}} - \lambda_{\mathrm{measured}}\right)^2}{\sum \left(\lambda_{\mathrm{estimated}} - \frac{1}{N}\sum \lambda_{\mathrm{estimated}}\right)^2} \tag{14}$$

where N is the number of data points, and p is the number of model parameters, and $\lambda_{estimated}$ and $\lambda_{measured}$ are the model estimates and measured values, respectively.

3. Results and discussion

3.1. Soil textural groups

It is well known that the thermal conductivity functions, expressed as normalized thermal conductivity (K_e) with respect to the degree of saturation (S_r), are influenced by the grain-size distribution of soils (Kersten 1949; Johansen 1975; Côté and Konrad, 2005a; Lu et al., 2007). Thus, it is unsurprising that previous studies often divided soils into different textural groups. For example, Johansen (1975) derived K_e functions in terms of S_r for fine- and coarse-textured soils, respectively. Côté and Konrad (2005a) obtained the best-fitted κ values for gravel and coarse sand, medium and fine sand, and silty and clayey soils, respectively. However, these studies do not define explicitly the boundary

Table 2
Soil ID, texture, particle size distribution, quartz content, porosity (ϕ) and sources of soils in the validation dataset including 58 soil samples.

Soil ID	Texture	Particle size distribution	Quartz content	ϕ	Sources		
		Sand	Silt	Clay		$cm^3\ cm^{-3}$	
42	silt loam	0.33	0.57	0.10	0.51	0.55	Tarnawski et al. (2015)
43	sandy loam	0.61	0.34	0.05	0.61	0.45	Tarnawski et al. (2015)
44	sandy loam	0.57	0.37	0.06	0.63	0.40	Tarnawski et al. (2015)
45	sand	1.00	0.00	0.00	1.00	0.36	Tarnawski et al. (2015)
46	loamy sand	0.85	0.12	0.03	0.72	0.40	Tarnawski et al. (2015)
47	sandy loam	0.56	0.38	0.06	0.72	0.51	Tarnawski et al. (2015)
48	silt loam	0.22	0.66	0.12	0.34	0.57	Tarnawski et al. (2015)
49	loam	0.5	0.42	0.08	0.66	0.44	Tarnawski et al. (2015)
50	loam	0.51	0.40	0.09	0.58	0.42	Tarnawski et al. (2015)
51	loamy sand	0.83	0.14	0.03	0.54	0.41	Tarnawski et al. (2015)
52	silt loam	0.03	0.82	0.15	0.57	0.54	Tarnawski et al. (2015)
53	silt loam	0	0.83	0.17	0.56	0.45	Tarnawski et al. (2015)
54	silt loam	0.24	0.66	0.1	0.55	0.62	Tarnawski et al. (2015)
55	silt loam	0.26	0.64	0.1	0.60	0.54	Tarnawski et al. (2015)
56	silty clay loam	0	0.67	0.33	0.38	0.54	Tarnawski et al. (2015)
57	sand	0.93	0.05	0.02	0.35	0.43	Tarnawski et al. (2015)
58	loamy sand	0.79	0.17	0.03	0.42	0.48	Tarnawski et al. (2015)
59	silt loam	0.36	0.56	0.08	0.28	0.43	Tarnawski et al. (2015)
60	silt loam	0.07	0.75	0.18	0.17	0.51	Tarnawski et al. (2015)
61	sandy loam	0.71	0.25	0.04	0.41	0.46	Tarnawski et al. (2015)
62	sand	0.89	0.10	0.01	0.38	0.39	Tarnawski et al. (2015)
63	sandy loam	0.56	0.37	0.07	0.36	0.38	Tarnawski et al. (2015)
64	loamy sand	0.84	0.14	0.02	0.38	0.44	Tarnawski et al. (2015)
65	silt loam	0.32	0.54	0.14	0.25	0.45	Tarnawski et al. (2015)
66	silt loam	0.17	0.69	0.14	0.38	0.55	Tarnawski et al. (2015)
67	silt loam	0.22	0.55	0.23	0.20	0.41	Tarnawski et al. (2015)
68	silt loam	0.03	0.76	0.21	0.21	0.63	Tarnawski et al. (2015)
69	loamy sand	0.81	0.16	0.03	0.61	0.47	Tarnawski et al. (2015)
70	silt loam	0	0.74	0.26	0.48	0.41	Tarnawski et al. (2015)
71	sandy loam	0.67	0.27	0.06	0.61	0.45	Tarnawski et al. (2015)
72	silt loam	0.02	0.83	0.15	0.37	0.53	Tarnawski et al. (2015)
73	loamy sand	0.83	0.14	0.03	0.67	0.42	Tarnawski et al. (2015)
74	sandy loam	0.68	0.27	0.05	0.63	0.45	Tarnawski et al. (2015)
75	silt loam	0.38	0.52	0.1	0.55	0.55	Tarnawski et al. (2015)
76	silty clay	0	0.58	0.42	0.21	0.51	Tarnawski et al. (2015)
77	silty clay	0	0.58	0.42	0.19	0.50	Tarnawski et al. (2015)
78	silty clay loam	0	0.70	0.30	0.27	0.51	Tarnawski et al. (2015)
79	silty clay	0	0.59	0.41	0.17	0.52	Tarnawski et al. (2015)
80	silty clay loam	0	0.67	0.33	0.17	0.53	Tarnawski et al. (2015)
81	silt loam	0.32	0.58	0.1	0.37	0.52	Tarnawski et al. (2015)
82	sand	0.91	0.03	0.06	–	0.47, 0.43, 0.40	Fu et al. (2021)
83	sandy loam	0.52	0.36	0.12	–	0.53, 0.49, 0.45	Fu et al. (2021)
84	silt loam	0.34	0.53	0.13	–	0.57, 0.53, 0.49	Fu et al. (2021)
85	sand	1.00	0.00	0.00	–	0.43	Fu et al. (2021)
86	silt loam	0.21	0.67	0.12	–	0.6	Fu et al. (2021)
87	clay loam	0.24	0.49	0.27	–	0.55	Fu et al. (2021)
88	sand	1.00	0.00	0.00	0.69	0.4	Tokoro et al. (2016)
89	sandy clay loam	0.53	0.22	0.25	0.07	0.52	Tokoro et al. (2016)
90	sand	1.00	0.00	0.00	0.34	0.31	Tokoro et al. (2016)
91	silt loam	0.25	0.58	0.17	–	0.44	Hailemariam et al. (2017)
92	silt loam	0.27	0.53	0.20	–	0.46	Hailemariam et al. (2017)
93	silt loam	0.10	0.65	0.25	–	0.48	Hailemariam et al. (2017)
94	sand	1.00	0.00	0.00	0.87	0.4	Tarnawski and Leong (2016)
95	clay	0.34	0.23	0.43	0.58	0.6	Tarnawski and Leong (2016)
96	silt loam	0.28	0.58	0.14	0.45	0.65	Tarnawski and Leong (2016)
97	sand	0.92	0.05	0.03	0.52	0.42	Tarnawski and Leong (2016)
98	loamy sand	0.71	0.26	0.03	–	0.44, 0.5	McCombie et al. (2016)
99	sand	0.91	0.07	0.02	–	0.45	Cass et al. (1981)

between each textural group, which can lead to improper selections of κ in Eq. (7) (He et al., 2017; Lu et al., 2007). He et al. (2021b) summarized detailed standards used in earlier studies to distinguish various texture groups.

Figure 4 presents the K_e values as a function of S_r for the 41 soils in the calibration dataset using six different classifications. Details of these classifications can be found in Table 3. Overall, three of six classifications divide soils into coarse-textured and fine-texture soils depending on sand or clay content. Among them, the division suggested by Johansen (1975) is the worst as the distribution of $K_e(S_r)$ curves for fine-textured soils are too scattered. The classification results by Kersten (1949) and Lu et al. (2007) are quite similar, because they used similar sand contents, 0.5 and 0.4, respectively, as the boundary. As expected, the coarse-textured soils show a more drastic increase of λ in the pendular regime (where discrete menisci are formed, and individual water bridges are built near particle contacts) and larger λ values than do the fine-textured soils over the range of saturations. In contrast, the fine-textured soils exhibit long flat tails at low S_r and delay the onset of the rapid increases in λ as S_r increases. This is because, compared to the coarse-textured soils, fine-textured soils have larger surface area and, thus, hold more water on the solid surfaces. Changes in the water content due to hydration result in small variations in heat transfer paths and, therefore, thermal conductivity (Lu and Dong, 2015). However, even in Figs. 4a and 4e, compared to the fine-textured soils, the

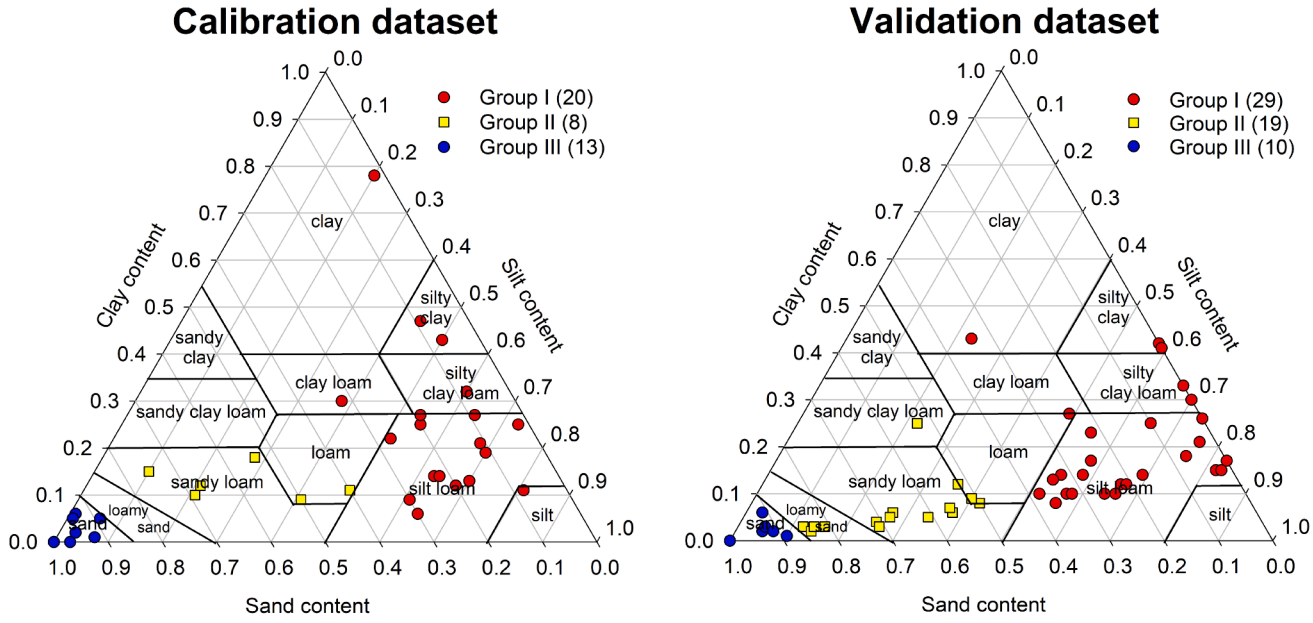

Fig. 3. Texture classes of the soils in the calibration and validation datasets. The number represents the number of soils in each textural group.

measured values of coarse-textured soils are more scattered, possibly due to the wider range of sand contents. Cox et al. (1999) and Côté and Konrad (2005a) separated soils into fine-, medium- and coarse-textured soils. However, the former approach resulted in a wide distribution of $K_e(S_r)$ curves for coarse-textured soils but a limited number for fine-textured soils (3); in contrast, the latter obtained 25 fine-textured soils but only 4 medium-textured soils. Overall, none of these five studies give satisfactory classification results. In this study, we recommend dividing the soil samples into three textural groups: Group I ($f_{sand} < 0.4$), Group II (other than Groups I and III), and Group III (sand). Group I represents fine-textured soils, and Group III only includes sand soils. Soils in Group II show intermediate characteristics between typical coarse- and fine-textured soils. Overall, there are 20 soils in Group I, 8 soils in Group II, and 13 soils in Group III in the calibration dataset. In the validation dataset, the number of soil samples in Groups I, II and III are 29, 19, and 10, respectively. Obviously, compared with the classifications discussed above, the group boundary values used in this study give a fairly uniform classification, and thus result in concentrated distributions of $K_e(S_r)$ curves in each textural group.

3.2. Model performances before calibration

Figure 5 compares λ values estimated via the three models against the measured values for the 58 soils in the validation dataset. The MAE, RMSE, and R^2 values were < 0.105 W m^{-1} K^{-1}, < 0.08 W m^{-1} K^{-1}, and > 0.95, respectively, for the C&K and Lu models. Both models provided quite accurate λ estimates. The G&D model with MAE = 0.125 W m^{-1} K^{-1}, RMSE = 0.089 W m^{-1} K^{-1}, and $R^2 = 0.95$ was slightly less accurate than the C&K and Lu models.

The C&K model performed better than the Lu model for soils in Group I. This differed from Lu et al. (2007) and Dong et al. (2015) who reported that the Lu model better described the λ-θ curve, especially for fine-textured soils. Fu and Horton (in review) found that the Lu model used a relatively low α parameter value (i.e., 0.27) for fine-textured soils, which enabled a good model performance at low S_r values but had poorer accuracy at intermediate saturation values. Among the three models, the G&D model performed best on Group III soils but worst on Group I and Group II soils (Table 4).

Measurements from a range of additional soil samples confirmed these findings. We determined the value of θ_c and t_s by fitting Eq. (2) to the data from Soils 1–41 then linked them to the f_{clay} (Fig. 6). Interestingly, we found a linear relationship between θ_c and f_{clay}, similar to Eq. (5). Our new coefficient and intercept values (i.e., 0.31 and 0.02) were close to 0.33 and 0 in Eq. (5) reported by Sadeghi et al. (2018) based on Soils 1–13. However, Fig. 6c is more scattered compared to Fig. 6a. Even after excluding an outlier, we found that the R^2 of 0.66 was lower than that for the original Sadeghi et al. (2018) coefficients. The t_s relationship with the f_{clay} ($R^2 = 0.01$) was weak. Thus, it is essential to calibrate the G&D model using the soils in the calibration dataset. For fair comparison, we also calibrated the C&K and Lu models using the same data. Because the relationships between parameters of the G&D model and clay content were not strong, we chose to determine the fitting θ_c and t_s values for the three soil groups as we did for the C&K and Lu models.

3.3. Determination of parameters after calibration

The three models were fitted to all the λ-θ curves in each group to determine the model fitting parameters. Table 5 summarizes the parameters for the three models before and after calibration. Before calibration, the C&K and Lu models have fitting values for each textural group to represent the parameters. In contrast, the parameters of the G&D model are dependent on the clay content as reported by Sadeghi et al. (2018).

For the C&K model, fitted κ values after calibration were 1.64 for Group I soils, 2.17 for Group II soils and 5.41 for Group III soils. It was not surprising that Group III had the largest κ value as large κ led to large λ at a given S, which was typical for coarse soils. For the Lu model, Group II soils and Group III soils yielded α and β values similar to the original values from the earlier calibrations. The Group I α value is 0.59 after calibration, which is more than twice the value reported by Lu et al. (2007). Recall that the Lu et al. (2007) α value of 0.27, determined on only four fine-textured soils, was found to be low leading to overestimations of λ, especially at medium saturation values (Fu and Horton, in review). Through calibration of the G&D model using 41 soils, the θ_c and t_s values were determined. We found $\theta_c = 0.08$ and $t_s = 0.385$ for Group I soils, $\theta_c = 0.03$ and $t_s = 0.415$ for Group II soils, and $\theta_c = 0.01$ and $t_s = 0.276$ for Group III soils. Among the three groups, Group I had the highest θ_c value, indicating that the amount of water required to

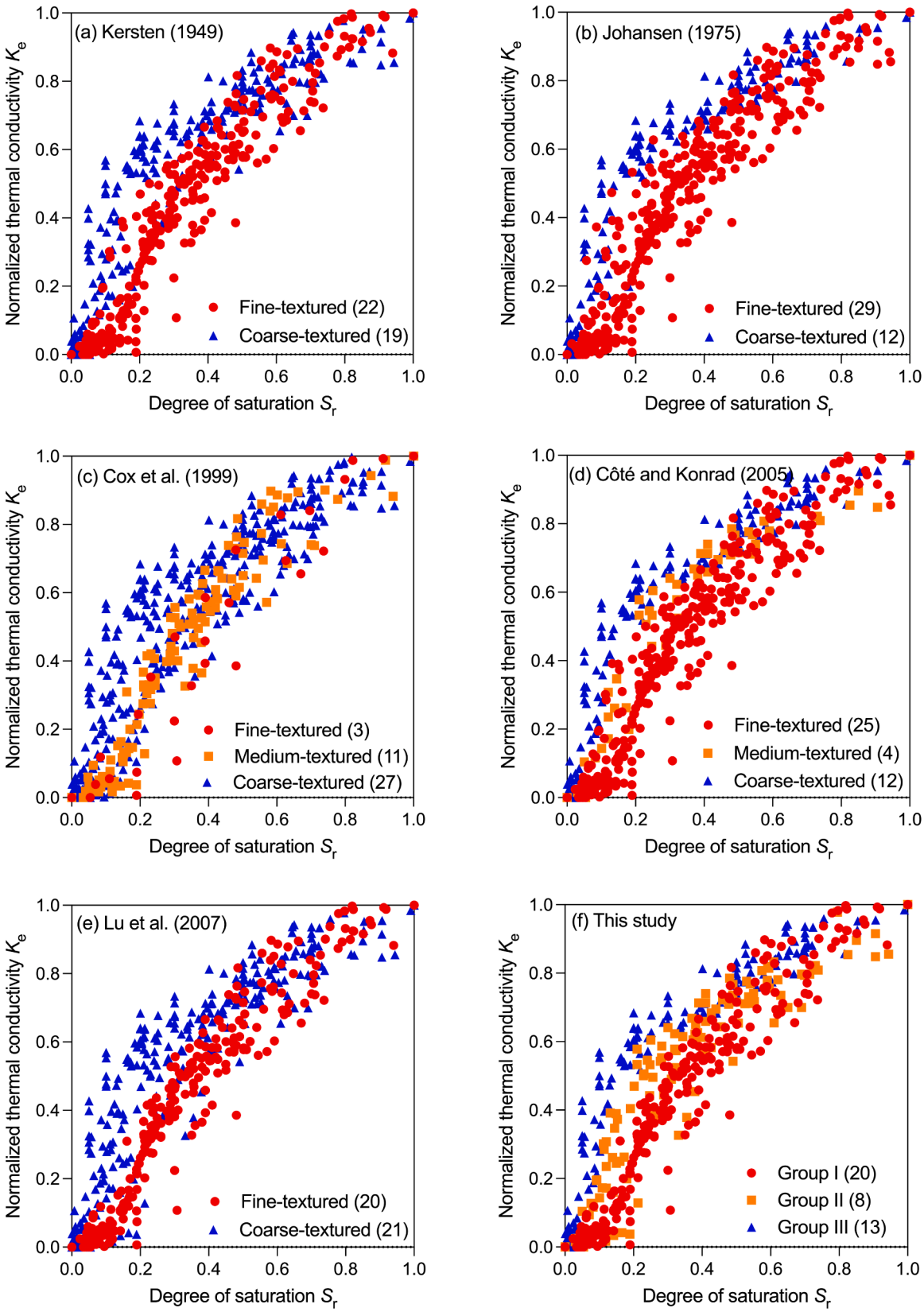

Fig. 4. Normalized thermal conductivity (K_e) as a function of degree of saturation (S) for Soils 1–41 in the calibration dataset. In each subplot, soils are separated into two or three groups according to the classification suggested by six different studies. The subplot (f) represents the classification used in this study: soils are classified into three groups: Group I ($f_{sand} < 0.4$), Group II (remainder) and Group III (sand). The number represents the number of soils in each textural group.

Table 3
The statistical results of each textural group using Soils 1–41 after six different classifications.

		Note	N	Average f_{sand}	Average f_{clay}
Kersten (1949)	Fine-textured	$f_{sand} \leq 0.5$	22	0.18	0.24
	Coarse-textured	$f_{sand} > 0.5$	19	0.85	0.05
Johansen (1975)	Fine-textured	$f_{clay} \leq 0.05$	29	0.30	0.21
	Coarse-textured	$f_{clay} > 0.05$	12	0.97	0.02
Cox et al. (1999)	Fine-textured	$f_{clay} \geq 0.35$ and $f_{silt} \leq 0.65$	3	0.05	0.56
	Medium-textured	Remainder	11	0.18	0.25
	Coarse-textured	$f_{sand} \geq 0.65$ or $f_{clay} \leq 0.18$	27	0.67	0.07
Côté and Konrad (2005a)	Fine-textured	$f_{sand} < 0.60$	25	0.22	0.23
	Medium-textured	$0.60 \leq f_{sand} < 0.90$	4	0.75	0.22
	Coarse-textured	$f_{sand} \geq 0.90$	12	0.97	0.02
Lu et al. (2007)	Fine-textured	$f_{sand} < 0.40$	20	0.16	0.25
	Coarse-textured	$f_{sand} \geq 0.40$	21	0.81	0.07
This study	Group I	$f_{sand} < 0.4$	20	0.16	0.25
	Group II	Remainder	8	0.56	0.14
	Group III	Sand	13	0.96	0.02

form a continuous heat flow path through the water phase was considerable. This was consistent with the fact that among the three groups, Group I had the highest average f_{clay} value (i.e., 0.25), thus likely the largest surface area. A positive correlation between the critical water content and surface area was experimentally reported by Moldrup et al. (2001). The fitted t_s values did not show any relationship with clay content. Group II had the highest t_s of 0.415 followed by 0.385 of Group I and 0.276 of Group III.

3.4. Model comparisons after calibration

Using the calibration optimized model parameters, we compared the performances of the three models. Fig. 7 shows the estimated λ values versus the measured ones for Soils 42–99 in the validation dataset after calibration. Overall, all three models provided accurate estimates, and RMSEs ranged from 0.086 to 0.096 W^{-1} m^{-1} K^{-1}, MAEs from 0.063 to 0.071 W^{-1} m^{-1} K^{-1}, and R^2 values were around 0.97. Based on Figs. 5 and 7 all three model performances improved after calibration. However, the extent of improvement among the models differed. The G&D model improved the most, and RMSE decreased by 26.4% and MAE by 24.7%. The C&K model improved the least, and RMSE and MAE decreased by only 6.8% and 5.3%, respectively. The C&K model's hyperbolic function did not capture the sigmoidal shape of the λ(θ) curve well. The Lu model performed best on Group I soils and Group II soils, and the G&D model performed best on Group III soils. Overall, after calibration, the G&D model performance was similar to the C&K and Lu models. This is a somewhat surprising and favorable result, as the capability of most theoretical λ(θ) models is generally limited due to simplified and idealized soil structure assumptions (Wang and Pan, 2008). This was especially noteworthy because the C&K and Lu models were the best performing models among a group of empirical models (Barry-Macaulay et al., 2015; He et al., 2020; Zhang and Wang, 2017). The C&K and Lu model parameters are empirical, which restricts their application other than to predict heat conduction in soils. In contrast, the theoretical foundation of the G&D model enables the model parameters (θ_c and t_s) to have physical meanings. Ghanbarian and Daigle (2016) proposed that θ_c could be roughly estimated from the residual water content (θ_r) and that the scaling exponent t_s could be related to the fractal dimension of the solid matrix or pore space. Therefore, the G&D model parameters are expected to be related to soil hydraulic properties and should be further investigated in future studies.

3.5. Further discussion

Although 99 soils covering 11 major textural classes (all except for sandy clay) are used in this study to calibrate and validate the performances of the G&D model and two other empirical models, there are only a few clay soils and no peat soils. Clay soils are different from other soils in many aspects, e.g., smaller particle size and higher specific surface area, which significantly affect the heat transfer process within the soils (Liu et al., 2021). For example, in clay soils where clay minerals (e.g., kaolinite, or magnetite and hematite) are predominant, quartz content is low. Eq. (9), which has been widely used in many previous studies to estimate the λ_{sat} values, may yield differences of up to 50% compared to measured values for 0% quartz content soils (Côté and Konrad, 2005b). Compared with mineral soils, peat soils have much higher organic matter content and are easily affected by soil shrinkage, which, however, received limited consideration (Zhao and Si, 2019). Zhao et al. (2019) developed a thermal conductivity model for peat soils

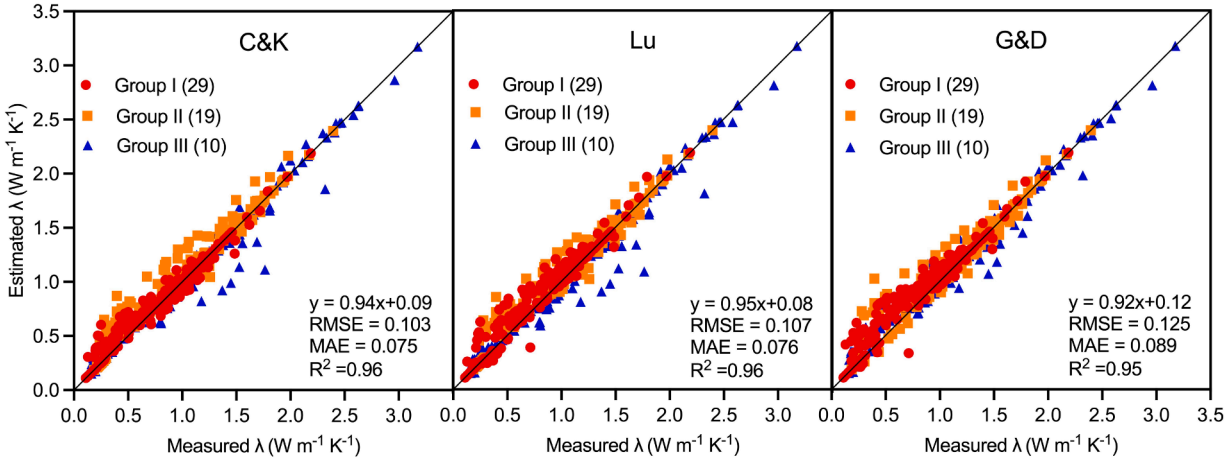

Fig. 5. Comparison of the C&K model, Lu model and G&D model λ values versus measured values for Soils 42–99 before calibration. The solid lines are the 1:1 lines. Groups I, II and III represent soils with $f_{sand} < 0.4$, $0.4 \leq f_{sand} < 1$ and $f_{sand} = 1$, respectively. The number represents the number of soils in each textural group.

Table 4
Validation results of Soils 42–99 for the C&K model, Lu model, and G&D model before and after calibration. Group I, II and III represent soils with $f_{sand} < 0.4$, remainder and sand, respectively. The superscript numbers represent the order of performance (e.g., 1 indicates the best and 3 indicates the worst).

	Parameters	Before calibration			After calibration		
		Group I	Group II	Group III	Group I	Group II	Group III
		$N = 29$	$N = 19$	$N = 10$	$N = 29$	$N = 19$	$N = 10$
C&K	RMSE	0.084^{1}	0.126^{2}	0.111^{2}	0.077^{3}	0.101^{3}	0.135^{3}
	MAE	0.061^{1}	0.092^{2}	0.079^{2}	0.056^{3}	0.073^{3}	0.105^{3}
	R^2	0.97^{1}	0.95^{2}	0.97^{2}	0.97^{3}	0.96^{3}	0.97^{3}
Lu	RMSE	0.096^{2}	0.118^{1}	0.115^{3}	0.066^{1}	0.093^{1}	0.128^{2}
	MAE	0.070^{2}	0.082^{1}	0.082^{3}	0.048^{1}	0.068^{1}	0.094^{2}
	R^2	0.95^{2}	0.95^{1}	0.97^{3}	0.97^{1}	0.97^{1}	0.97^{2}
G&D	RMSE	0.127^{3}	0.135^{3}	0.103^{1}	0.075^{2}	0.097^{2}	0.124^{1}
	MAE	0.092^{3}	0.092^{3}	0.078^{1}	0.054^{2}	0.072^{2}	0.090^{1}
	R^2	0.94^{3}	0.94^{3}	0.97^{1}	0.96^{2}	0.97^{2}	0.97^{1}

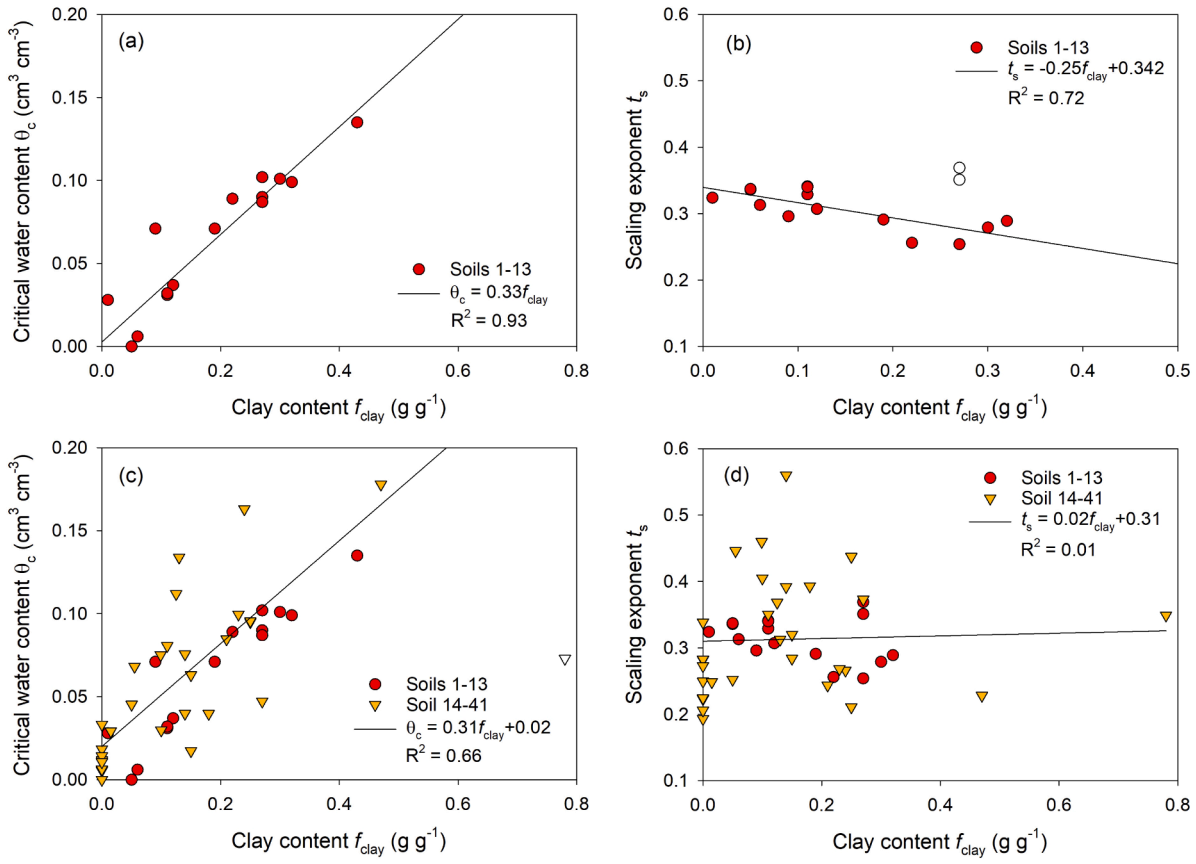

Fig. 6. Parameters θ_c and t_s of the G&D model as a function of clay content (f_{clay}) for Soils 1–13 (6a-6b) or Soils 1–41 (6c-6d). The solid lines represent the regression lines and white symbols identify outliers in subplots 6b and 6c.

Table 5
Best fitting parameters of the C&K model, the Lu model, and the G&D model before and after calibration using Soils 1–41 in this study.

	Parameters	Before calibration		After calibration		
		Fine-textured	Coarse-textured	Group I	Group II	Group III
		$N = 20$	$N = 21$	$N = 20$	$N = 8$	$N = 13$
C&K	κ	1.9	3.55	1.64	2.17	5.41
Lu	α	0.27	0.96	0.59	1.05	0.94
	β	1.33	1.33	1.35	1.48	1.23
G&D	θ_c	$\theta_c = 0.33 f_{clay}$		0.08	0.03	0.01
	t_s	$t_s = -0.25 f_{clay} + 0.342$		0.385	0.415	0.276

by assuming a universal logarithmic function between K_e and S_r (i.e., $K_e = \log_2(1 + S_r)$), which needed only λ_{dry} and λ_{sat} as inputs and performed well on peat soils. However, their model is not suitable for other types of soils as the shape of K_e with respect to S_r curves depends on soil texture, and thus cannot be represented by a universal function. In summary, additional soil types, particularly clay and peat soils, are needed in future studies to further evaluate and improve the performance of the G&D model.

In this study, we used measured λ_{dry} and λ_{sat} values rather than estimated results to avoid the potential influences on the calibration accuracy. For practical application, it would be valuable to further examine the performance of G&D model in conjunction with the models for estimating the λ_{dry} and λ_{sat}. However, as reviewed by He et al. (2021a) and Wang et al. (2020), there have been a large number of λ_{dry}

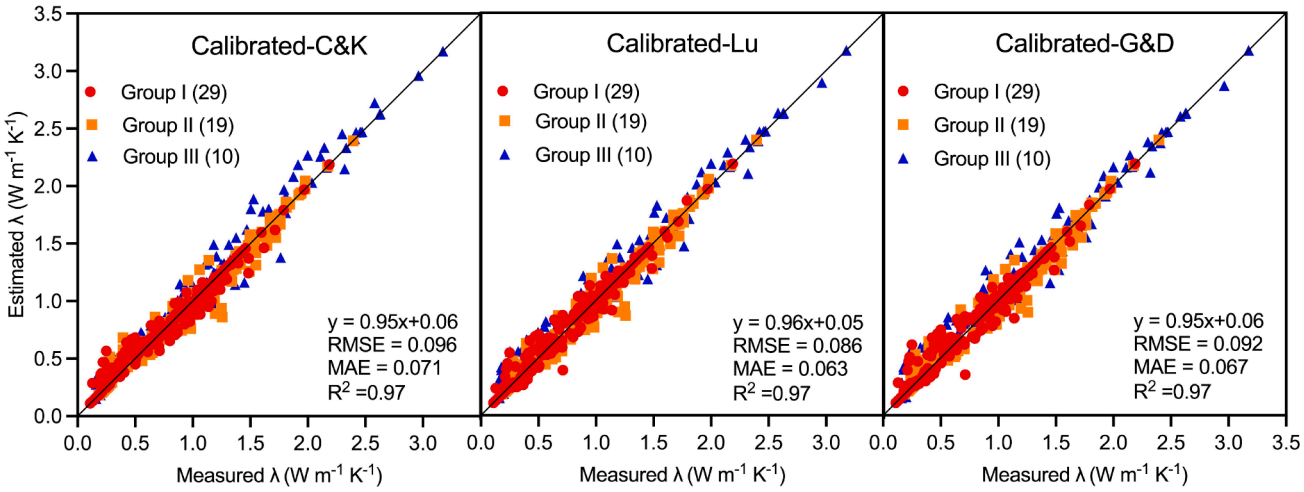

Fig. 7. Comparison of C&K, Lu, and G&D model estimated λ values versus the measured values for Soils 42–99 after calibration. The solid lines indicate the 1:1 line. The number represents the number of soils in each textural group.

and λ_{sat} models but none of them consistently provided accurate estimates. For example, Eq. [9], the geometric mean method, provided the best λ_{sat} estimates, but it required complete mineral composition information, thus making it impractical to apply. Thus, it is essential to develop a new model for estimating λ_{sat} with attainable soil properties rather than mineral composition in the future.

4. Conclusion

Although there exist numerous empirical thermal conductivity models in the literature, the number of theoretical models is very limited. One theoretical approach, the G&D model, is based on the percolation-based effective-medium approximation, which encompasses several other existing models as its special cases. In this study, we calibrated the parameters of the theoretical G&D model and two other empirical λ(θ) models using a dataset of 41 soils. For this purpose, three soil groups based on the sand content were defined (Group I: $f_{sand} < 0.4$, Group II: other than Groups I and III, and Group III: sand). After calibration, the performances of the three λ(θ) models were evaluated using an independent dataset including 58 soil samples. The performances of all of the calibrated models improved compared to the original models, and they provided accurate estimations of measured λ values in an independent validation dataset. More importantly, the G&D model has two physically-meaningful parameters, i.e., critical water content (θ_c) and scaling exponent (t_s) which may be estimated from residual water content and fractal dimension of the solid matrix or pore space, respectively, as suggested by Ghanbarian and Daigle (2016). Once these correlations were developed, the robust performance after calibration in this study provided the basis to further establish pedo-transfer functions to estimate the soil hydraulic properties from λ(θ) measurements or basic soil properties (e.g., texture and porosity).

Declaration of Competing Interest

The authors declare that they have no known competing financial interests or personal relationships that could have appeared to influence the work reported in this paper.

Data availability

Data will be made available on request.

Acknowledgements

This research was supported by the US National Science Foundation (Grant Number: 2037504) and USDA-NIFA Multi-State Project 4188. Behzad Ghanbarian is grateful to Kansas State University for financial support through a faculty startup fund.

References

Abu-Hamdeh, N.H., Reeder, R.C., 2000. Soil thermal conductivity effects of density, moisture, salt concentration, and organic matter. Soil Sci. Soc. Am. J. 64 (4), 1285–1290.
Barry-Macaulay, D., Bouazza, A., Wang, B., Singh, R.M., 2015. Evaluation of soil thermal conductivity models. Can. Geotech. J. 52 (11), 1892–1900.
Campbell, G.S., Jungbauer, J.D., Bidlake, W.R., Hungerford, R.D., 1994. Predicting the effect of temperature on soil thermal conductivity. Soil Sci. 158 (5), 307–313.
Cass, A.G., Campbell, G.S., Jones, T.L., 1981. Hydraulic and thermal properties of soil samples from the buried waster test facility. PNL-4015, Pacific Northwest Laboratory, Richland.
Chen, S.X., 2008. Thermal conductivity of sands. Heat Mass Transf. 44 (10), 1241–1246.
Côté, J., Konrad, J.-M., 2005a. A generalized thermal conductivity model for soils and construction materials. Can. Geotech. J. 42 (2), 443–458.
Côté, J., Konrad, J.-M., 2005b. Thermal conductivity of base-course materials. Can. Geotech. J. 42 (1), 61–78.
de Vries, D.A., 1963. Thermal properties of soils. In: van Wijk, W.R. (Ed.), Physics of Plant Environment. North-Holland Publishing Company, Amesterdam, pp. 210–235.
Donazzi, F., Occhini, E., Seppi, A., 1979. Soil thermal and hydrological characteristics in designing underground cables. Proc. Institution Electr. Eng. 126 (6), 506.
Dong, Y.i., McCartney, J.S., Lu, N., 2015. Critical review of thermal conductivity models for unsaturated soils. Geotechnical Geological Eng. 33 (2), 207–221.
Fu, Y., Horton, Heitman, J.L. (in review). A new closed-form soil thermal conductivity model for improved prediction at low and medium range of saturation.
Fu, Y., Horton, R., Ren, T., Heitman, J.L., 2021. A general form of Archie's model for estimating bulk soil electrical conductivity. J. Hydrol. 597, 126160.
Ghanbarian, B., Daigle, H., 2016. Thermal conductivity in porous media: Percolation-based effective-medium approximation. Water Resour. Res. 52 (1), 295–314.
Gori, F., Corasaniti, S., 2013. New model to evaluate the effective thermal conductivity of three-phase soils. Int. Commun. Heat Mass 47, 1–6.
Haigh, S.K., 2012. Thermal conductivity of sands. Géotechnique 62 (7), 617–625.
He, H., Zhao, Y., Dyck, M.F., Si, B., Jin, H., Lv, J., Wang, J., 2017. A modified normalized model for predicting effective soil thermal conductivity. Acta Geotech. 12 (6), 1281–1300.
He, H., Noborio, K., Johansen, Ø., Dyck, M.F., Lv, J., 2020. Normalized concept for modelling effective soil thermal conductivity from dryness to saturation. Eur. J. Soil Sci. 71, 27–43.
He, H., Liu, L., Dyck, M., Si, B., Lv, J., 2021a. Modelling dry soil thermal conductivity. Soil Tillage Res. 213, 105093.
Hailemariam, H., Shrestha, D., Wuttke, F., Wagner, N., 2017. Thermal and dielectric behaviour of fine-grained soils. Environmental Geotechnics 4, 79–93.
He, H., Flerchinger, G.N., Kojima, Y., Dyck, M., Lv, J., 2021b. A review and evaluation of 39 thermal conductivity models for frozen soils. Geoderma 382, 114694.
Hopmans, J.W., Dane, J.H., 1986. Thermal conductivity of two porous media as a function of water content, temperature, and density. Soil Sci. 142 (4), 187–195.

Horai, K.-I., 1971. Thermal conductivity of rock-forming minerals. J. Geophys. Res. 76 (5), 1278–1308.
Jia, G.S., Tao, Z.Y., Meng, X.Z., Ma, C.F., Chai, J.C., Jin, L.W., 2019. Review of effective thermal conductivity models of rock-soil for geothermal energy applications. Geothermics 77, 1–11.
Johansen, Ø., 1975. Thermal conductivity of soils. Ph.D. thesis. University of Trondheim. US Army Corps of Engineers, Cold Regions Research and Engineering Laboratory, Hanover, N. H. CRREL Draft English Translation 637, Trondheim, Norway.
Kersten, M.S, 1949. Laboratory research for the determination of the thermal properties of soils. Research Laboratory Investigations, Engineering Experiment Station, Technical Report 23, University of Minnesota, Minneapolis, Minn.
Liu, L., He, H., Dyck, M., Lv, J., 2021. Modeling thermal conductivity of clays: a review and evaluation of 28 predictive models. Eng. Geol. 288, 106107.
Lu, S., Ren, T., Gong, Y., Horton, R., 2007. An improved model for predicting soil thermal conductivity from water content at room temperature. Soil Sci. Soc. Am. J. 71 (1), 8–14.
Lu, S., Ren, T., Yu, Z., Horton, R., 2011. A method to estimate the water vapour enhancement factor in soil. Eur. J. Soil Sci. 62, 498–504.
Lu, Y., Wang, Y., Ren, T., 2013. Using late time data improves the heat-pulse method for estimating soil thermal properties with the pulsed infinite line source theory. Vadose Zone J. 12, 1–9.
McCombie, M.L., Tarnawski, V.R., Bovesecchi, G., Coppa, P., Leong, W.H., 2016. Thermal conductivity of Pyroclastic Soil (Pozzolana) from the environs of Rome. Int. J. Thermophys. 38, 21.
McInnes, K.J., 1981. Thermal conductivities of soils from dryland wheat regions of Eastern Washington (Master dissertation). Washington State University, Pullman, WA.
McLachlan, D.S., 1987. An equation for the conductivity of binary mixtures with anisotropic grain structures. J. Phys. C Solid State Phys. 20 (7), 865–877.
Moldrup, P., Olesen, T., Komatsu, T., Schjønning, P., Rolston, D.E., 2001. Tortuosity, diffusivity, and permeability in the soil liquid and gaseous phases. Soil Sci. Soc. Am. J. 65 (3), 613–623.
Sadeghi, M., Ghanbarian, B., Horton, R., 2018. Derivation of an explicit form of the percolation-based effective-medium approximation for thermal conductivity of partially saturated soils. Water Resour. Res. 54 (2), 1389–1399.
Shiozawa, S., Campbell, G.S., 1990. Soil thermal conductivity. Remote Sens Rev 5 (1), 301–310.
Tarnawski, V.R., Leong, W.H., 2016. Advanced geometric mean model for predicting thermal conductivity of unsaturated soils. Int. J. Thermophys. 37, 18.
Tarnawski, V.R., McCombie, M.L., Momose, T., Sakaguchi, I., Leong, W.H., 2013. Thermal conductivity of standard sands. Part III. Full range of saturation. Int. J. Thermophys. 34 (6), 1130–1147.
Tarnawski, V.R., Momose, T., McCombie, M.L., Leong, W.H., 2015. Canadian field soils III. Thermal-conductivity data and modeling. Int. J. Thermophys. 36 (1), 119–156.
Tarnawski, V.R., McCombie, M.L., Leong, W.H., Coppa, P., Corasaniti, S., Bovesecchi, G., 2018. Canadian field soils IV: modeling thermal conductivity at dryness and saturation. Int. J. Thermophys. 39, 35.
Tokoro, T., Ishikawa, T., Shirai, S., Nakamura, T., 2016. Estimation methods for thermal conductivity of sandy soil with electrical characteristics. Soils Found. 56 (5), 927–936.
Tong, F., Jing, L., Zimmerman, R.W., 2009. An effective thermal conductivity model of geological porous media for coupled thermo-hydro-mechanical systems with multiphase flow. Int. J. Rock Mech. Min. 46 (8), 1358–1369.
Usowicz, B., Lipiec, J., Usowicz, J.B., Marczewski, W., 2013. Effects of aggregate size on soil thermal conductivity: comparison of measured and model-predicted data. Int. J. Heat Mass Tran. 57 (2), 536–541.
Wang, J., He, H., Li, M., Dyck, M., Si, B., Lv, J., 2020. A review and evaluation of thermal conductivity models of saturated soils. Arch. Agron. Soil Sci. 67 (7), 974–986.
Wang, M., Pan, N., 2008. Predictions of effective physical properties of complex multiphase materials. Mater. Sci. Eng. R Reports 63 (1), 1–30.
Woodside, W., Messmer, J.H., 1961. Thermal conductivity of porous media. I. Unconsolidated sands. J Appl Phys 32, 1688–1699.
Zhang, N., Wang, Z., 2017. Review of soil thermal conductivity and predictive models. Int. J. Therm. Sci. 117, 172–183.
Zhao, Y., Si, B., 2019. Thermal properties of sandy and peat soils under unfrozen and frozen conditions. Soil Tillage Res. 189, 64–72.
Zhao, Y., Si, B., Zhang, Z., Li, M., He, H., Hill, R.L., 2019. A new thermal conductivity model for sandy and peat soils. Agr. Forest Meteorol. 274, 95–105.